processes

MDPI

Article

Conversion of Carbonaceous Organic Impurities (Methyldichlorosilane) in Trichlorosilane Using Weakly Basic Anion-Exchange Resin as Solid Catalyst

Jianhua Liu, Miaolei Zhang and Guoqiang Huang *

School of Chemical Engineering and Technology, Tianjin University, Tianjin 300072, China
* Correspondence: hgq@tju.edu.cn

Abstract: Trichlorosilane ($SiHCl_3$) is an important raw material for preparing solar cells and semiconductor chips in the Siemens method. Since the boiling points of $SiHCl_3$ and methyldichlorosilane (CH_3SiHCl_2) are close to each other, it is difficult to remove CH_3SiHCl_2 from the raw material to obtain high-purity products by traditional distillation methods. Therefore, we propose an efficient catalytic approach to convert CH_3SiHCl_2 to methyltrichlorosilane (CH_3SiCl_3) with an anion-exchange resin as the catalyst and tetrachlorosilane ($SiCl_4$) as the Cl donor in a continuous-flow fixed bed reactor. Seven anion-exchange resins, including D201, D301, D303, 201 × 7, D301F, D315 and D380 were evaluated. The results showed that D301 resin had the best performance. Reaction conditions such as reaction temperature, reactant molar ratio and catalyst stability were investigated. The maximum conversion of CH_3SiHCl_2 was 60% at an optimum reaction temperature of 150 °C, $n(CH_3SiHCl_2):n(SiCl_4)$ = 1:3 and a liquid hourly space velocity (LHSV) of 3.0 h^{-1}. A possible reaction mechanism is explained based on the reaction data obtained in the current work.

Keywords: anion-exchange resin; de(hydro)halogenization; heterogeneous catalysis; methyldichlorosilane; tetrachlorosilane

Citation: Liu, J.; Zhang, M.; Huang, G. Conversion of Carbonaceous Organic Impurities (Methyldichlorosilane) in Trichlorosilane Using Weakly Basic Anion-Exchange Resin as Solid Catalyst. *Processes* **2023**, *11*, 429. https://doi.org/10.3390/pr11020429

Academic Editor: Christos Argirusis

Received: 11 December 2022
Revised: 21 January 2023
Accepted: 25 January 2023
Published: 31 January 2023

1. Introduction

The intensification of the global climate and energy crises has increased interest in green and sustainable energy. In recent years, the photovoltaic (PV) industry has grown rapidly, with total installed solar panel capacity growing at an annual rate of about 20–35% from 2013–2021. Global installed PV capacity will reach terawatt levels in the next few years [1,2]. One of the main raw materials for producing PV modules is polysilicon [3,4], which is used in the PV field to prepare solar cells, and the semiconductor industry also needs higher-purity polysilicon to prepare semiconductor chips. The primary process used to obtain polysilicon is the Siemens process [5–9], which is used by more than 80% of polysilicon manufacturers worldwide. It mainly involves the hydrochlorination of industrial silicon to trichlorosilane ($SiHCl_3$) and $SiHCl_3$ distillation, followed by the hydrogen reduction of the $SiHCl_3$ to polysilicon. It is challenging to remove carbon-containing impurities, which are generated during the hydrochlorination of low-purity industrial silicon with HCL, from $SiHCl_3$ in the $SiHCl_3$ distillation process, especially since the difference in boiling point (BP) between methyldichlorosilane (CH_3SiHCl_2) and $SiHCl_3$ at atmospheric pressure is only 8 °C ($SiHCl_3$ BP 33 °C; CH_3SiHCl_2 BP 41 °C). $SiHCl_3$ carrying these carbon-containing impurities will deposit carbon in polysilicon during the hydrogen reduction process, ultimately affecting the product's performance [10,11].

For CH_3SiHCl_2 removal, traditional means such as adsorption and distillation require high investment and energy consumption. Some improved distillation techniques such as dividing wall columns [12], heat pump distillation [13] and thermally coupled distillation [14] have been used to reduce energy consumption in recent years, but due to the nature of CH_3SiHCl_2, it is very difficult to completely remove CH_3SiHCl_2 from $SiHCl_3$

with traditional means. Catalytic chlorination is currently the most effective and least costly method compared with the above methods. This method introduces a chlorinating agent and catalyzes the reaction to convert CH_3SiHCl_2 to methyltrichlorosilane (CH_3SiCl_3), facilitating the subsequent purification of $SiHCl_3$. Several types of chlorinating agents, such as halogenated hydrocarbons and Cl_2, and catalysts have been used in similar reactions [15–18]. However, the introduction of substances outside the production system inevitably creates additional separation requirements. The use of the highly toxic and corrosive gas Cl_2 poses considerable problems for subsequent operational safety and the selection of equipment materials, and the improper use of these substances can also deplete the raw material $SiHCl_3$. $SiCl_4$ reduction is an important part of the polysilicon closed production loop. A key step is the reaction of $SiCl_4$ and H_2 to obtain $SiHCl_3$ [19]. This suggests that $SiCl_4$ can be used as a chlorinating agent to react with CH_3SiHCl_2. As an intermediate product, the introduction of $SiCl_4$ can also avoid the undesirable effects of the above-mentioned chlorinating agents.

We also note that the reaction can be carried out without catalysts only at 800 °C, and A.V. Vorotyntsev et al. [7] achieved the same effect at 250 °C by using nickel chloride as a catalyst. There is no doubt that proper catalysts can significantly improve catalytic efficiency. Some catalysts, such as Lewis acids and transition metal compounds [15,20], have been used in dechlorination hydrogenation reactions of halogenated hydrocarbons. However, almost all such catalysts introduce various impurities into the product. Ion-exchange resins are well known as solid catalysts with many advantages, such as cheap price, stable structure, safety and nontoxicity, high mechanical strength and corrosion resistance. They have been applied in biodiesel production [21,22] and organic synthesis [23–25]. Wu et al. [26] studied the esterification reaction of 4-methoxyphenylacetic acid with n-bromobutane in a dichloromethane/alkali two-phase reaction using two quaternary ammonium resins, a gel type and a microporous type, as the catalysts. The results of the reaction activation energy test showed that the microporous resin had a lower catalytic activation energy and a better catalytic effect than the gel-type resin. Yu et al. [27] prepared a graphene-reinforced anion-exchange resin using graphene as an enhancer, which could significantly improve the thermal stability performance of the resin. Mori et al. [28] found that novel catalysts prepared using resin-loaded metal Pd and Pd-Ag nanoparticles possess catalytic activity for the hydrogen production reaction by methanol decomposition. It was also found that there was a synergistic effect between the metal Pd particles loaded on the weakly basic tertiary amine resin and the tertiary amine group, which improved the catalytic activity. Although the catalytic role of anion-exchange resins has been well documented, in the field of organic reactions, they have been used mainly as solid base catalysts in esterification and ester exchange reactions [26,29,30]. Few researchers have focused on their role in the catalytic conversion of hydrogen-containing alkanes and hydrogen-containing silanes.

In this study, a practical method is proposed for converting CH_3SiHCl_2 to CH_3SiCl_3 using anion-exchange resins as the catalyst and $SiCl_4$ as the reactant. We compared the catalytic activity of various anion-exchange resins (resins with strongly basic functional groups in the form of chlorine with the presence of ammonium groups) and investigated the effects of reaction temperature, reactant ratio, liquid hourly space velocity (LHSV) and catalyst reuse on the catalytic reaction. This study will provide a better understanding of the conversion of hydrogen-containing silanes and the separation of high-purity substances.

2. Materials and Methods

2.1. Reagents and Materials

Methyldichlorosilane (CH_3SiHCl_2, 99.5%), methyl trichlorosilane (CH_3SiCl_3, 99%), trichlorosilane ($SiHCl_3$, 99.5%), and silicon tetrachloride ($SiCl_4$, 99.5%) were purchased from Macklin Reagent Company (Shanghai, China). Sodium hydroxide (NaOH, AR), hydrochloric acid (HCl, AR) and ethanol (CH_3CH_2OH, 99.99%) were purchased from Tianjin Yuanli Chemical Trading Ltd. (Tianjin, China). Hydrogen (H_2, 99.99%) and nitrogen (N_2, 99.99%) were purchased from Tianjin Air Liquide Ltd. (Tianjin, China). Deionized

water was purified with a QH water purification system from Qianhe Water Treatment Engineering Ltd. (Dongguan, China).

2.2. Treatment of Anion-Exchange Resins

D301 and D201 anion-exchange resins were purchased from Macklin Reagent Company (Shanghai, China), and 201 × 7, D301F, D303, D315 and D380 were purchased from Hecheng New Materials Ltd. (Zhengzhou, China). Table 1 lists their physical and chemical properties. Each of the anion-exchange resins was supplied in chloride form. Before use, the resin surface was repeatedly washed with ethanol until the filtrate became colorless and clear to remove monomers and pore-forming agents that had adhered to the pores during the synthesis process. The resin was then treated in turn with 1.0 mol/L NaOH and 1.0 mol/L HCL. After soaking/stirring, the resin was rewashed several times with deionized water until the filtrate was neutral. Finally, the resin was dried at 80 °C until its quality remained constant.

Table 1. Characteristics of anion-exchange resins used.

Resins	Character	Functional Groups	Particle Diameter (mm)	Moisture Content (%)	Exchange Capacity (meq g^{-1})
D301	M [1]	$-N(CH_3)_2$	0.32–1.25	48~58	4.9
D301F	M [1]	$-N(CH_3)_2$	0.45–1.25	50~60	4.8
D303	M [1]	$-N(CH_3)_2$	0.32–1.25	50~60	5.4
D315	M [1]	$-N(CH_2CH_2NH)_2$	0.45–1.25	55~65	6.2
D380	M [1]	$-NHCH_3$	0.32–1.25	52~60	4.3
D201	M [1]	$-N^+(CH_3)_3$	0.32–1.25	50~60	3.7
201 × 7	G [2]	$-N^+(CH_3)_3$	0.32–1.25	42~48	3.6

[1]. Macroreticular type. [2]. Gel type.

2.3. Instrumentation and Analytical Conditions

The experimental setup is shown in Figure 1. In addition to the corresponding equipment and its internal piping made of 304SS stainless steel, the piping and valves through which the reactants and products pass are all made of polytetrafluoroethylene, which is resistant to chlorides of silicon. Four mL of the catalyst was loaded into the thermostatic zone of the reactor (tubular type, 10 mm inner diameter, 450 mm long). Quartz wool was installed below the catalyst to fix it.

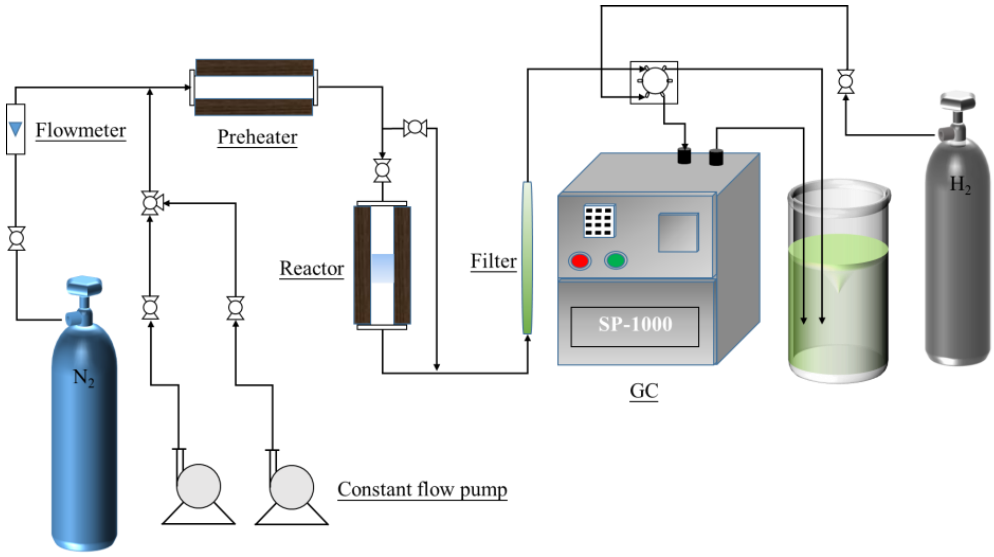

Figure 1. Apparatus for investigation of the catalytic conversion of CH_3SiHCl_2.

A programmed temperature rise controller controlled the temperature of the preheater and reactor. After reaching the set temperature, the carrier gas was turned on to purge all pipelines for 30 min and all experiments were carried out at a carrier gas flow rate of 15 mL/min.

CH_3SiHCl_2 and $SiCl_4$ were sent into the pipeline by two constant flow pumps, and the ratio of reactants was set by the flow rate of the constant flow pumps. The two reactants converged after the three-way valve and then entered the gasification chamber together with the carrier gas to form the feed gas at 80 °C in the reactor. The gas mixture from the reactor was analyzed with a gas chromatograph (GC SP-1000) equipped with a thermal conductivity detector (TCD) and a 6 m long OV-210 column packed with 50% polytrifluoropropyl(methyl)siloxane.

The following equation is used to quantify the conversion of CH_3SiHCl_2, which is used as a criterion for evaluating catalytic performance:

$$X = \frac{x(CH_3SiHCl_2)_{in} - x(CH_3SiHCl_2)_{out}}{x(CH_3SiHCl_2)_{in}} \quad (1)$$

$x(CH_3SiHCl_2)_{in}$ and $x(CH_3SiHCl_2)_{out}$ are defined as the mole fractions of CH_3SiHCl_2 at the reactor's inlet and outlet.

2.4. Determination of Tertiary Amine Group Content on Resin Surfaces

There is a pair of unshared electrons on the nitrogen atom of the amine group, so the amine group can combine with a proton to form the ammonium ion:

$$R - NH_2 + H^+ \rightarrow R - N^+H_3 \quad (2)$$

After drying the anion-exchange resin, 2.00 g of the dried resin was weighed, 150 mL of 0.3 mol/L HCl standard solution was added, the solution was shaken in a constant temperature water bath for 8 h, 5 mL of the supernatant was removed, and 10 mL of deionized water and 3 drops of 0.1% methyl orange indicator was added. The solution was titrated with 0.1 mol/L NaOH standard solution; the endpoint was when the specimen turned from red to orange. The calculation formula is as follows.

$$\text{Amine group content}(\%) = \frac{C_1V_1 - C_2V_2}{G} \times 16 \times 100 \quad (3)$$

C_1—The concentration of HCl solution, mol/L
V_1—The amount of HCl solution, L
C_2—The concentration of NaOH solution, mol/L
V_2—The amount of NaOH solution, L
G—Sample mass, g

2.5. Catalyst Characterization

N_2 Adsorption–desorption isotherms and mesoporous structure data of the catalysts were obtained with a BELSORP Max II surface area and porosity analyzer (MicrotracBEL, Osaka, Japan). The new catalyst was evacuated in a vacuum chamber at 150 °C for 10 h. N_2 adsorption–desorption was carried out in a liquid nitrogen environment after cooling.

Samples were analyzed by TGA on a thermogravimetric TGA/DSC3 analyzer (Mettler, Greifensee, Switzerland). Then 5 mg of catalyst was weighed into an aluminum crucible and heated from 50 to 500 °C at a heating rate of 10 K/min and a flow rate of 50 mL/min in a nitrogen atmosphere.

The external and internal structures of the resins were investigated using an S-4800 scanning electron microscope (Hitachi, Tokyo, Japan). The resin was fixed on double-sided tape and gold-blasted using an E-1045 ion sputter (Hitachi, Tokyo, Japan). The maximum acceleration voltage was 15 KV and the secondary electron resolution was 1.0 nm.

TEM patterns were obtained using a JEM-F200 Transmission Electron Microscope (JEOL, Tokyo, Japan). Its accelerating voltage was 200 kV. The sample was ground into powder, added to ethanol and placed in the ultrasonic to make a suspension. A small amount of liquid was placed on the grating and the sample was prepared after the liquid drops evaporated completely.

The catalyst samples were measured by XRD using a SmartLab diffractometer (Rigaku, Tokyo, Japan) and a Cu-Kα monochromatic beamline (tube voltage 40 kV, tube current 40 mA). The step size was 0.02°, and the integration time was 2 s. The range of scan angles was 10° to 80°.

3. Results and Discussion

3.1. Comparison of Catalytic Performance of Different Catalysts

The catalytic activity of the resins was tested in the apparatus shown in Figure 1 under the above conditions, and the tests were performed according to the procedure described in Section 2.3. The catalytic activity of the resins was evaluated by CH_3SiHCl_2 conversion, and the results are shown in Table 2. It can be seen that the conversion of CH_3SiHCl_2 was significantly higher with D301, D301F and D303 resins than with the others. They showed good catalytic activity, with D301 resin showing the best performance in the CH_3SiHCl_2 conversion process. This result is related to the functional groups of the resin. The selection of a suitable resin should be based on the crosslinking density of the resin, as well as its ability to bind to the reactants, specific surface area, pore size, etc. The binding ability of the resin to the reactants is related to the electrostatic attraction between them and the hydrophobic interaction between the side chains and the resin matrix polystyrene [31].

Table 2. The results of reactor outlet components on different types of resins.

Resins	Low Boilers	CH_3SiH_2Cl (mol%)	CH_3SiHCl_2 (mol%)	$SiHCl_3$ (mol%)	$SiCl_4$ (mol%)	CH_3SiCl_3 (mol%)	Conversion (%)
D301	0.0	0.8	33.9	16.4	34.3	16.9	35.1
D301F	0.3	1.0	33.3	16.2	33.8	16.7	33.4
D303	0.0	0.6	37.3	12.7	37.8	12.7	25.4
D315	0.0	0.0	50.0	0.0	50.0	0.0	0.0
D380	0.0	0.0	50.0	0.0	50.0	0.0	0.0
D201	0.1	0.1	47.2	2.6	47.3	2.8	5.6
201X7	0.0	0.0	50.0	0.0	50.0	0.0	0.0

Temperature 100 °C, n($SiCl_4$):n(CH_3SiHCl_2) = 1:1, LHSV 1.5 h^{-1}.

3.2. Resin Characterization

3.2.1. Characterization of Pore and Surface Structure by Nitrogen Physisorption

To examine the pore structure, nitrogen adsorption–desorption isotherms were determined over the widest viable relative pressure range. The obtained isotherms were obtained for D301 resin, attributed to type II. The adsorption volume rises rapidly at lower relative pressures due to the strong adsorbent–adsorbate interaction. As shown in Figure 2, the desorption isotherm exhibits a distinct inflection point at P/P_0 = 0.05. This usually corresponds to the completion and termination of monolayer adsorption. Multilayer adsorption gradually forms as the relative pressure is further increased. A plateau does not form when the relative pressure reaches the saturation pressure.

The pore size distribution was obtained from the N_2 desorption isotherm using the Kelvin equation. Figure 3 shows the pore size distribution of D301 resin. This indicates that this resin contains a small amount of mesopores in addition to macropores. This explains why the adsorption and desorption isotherms did not fully overlap at higher relative pressures. However, the adsorption behavior indicates the macroporous structure of resin due to the lack of clear hysteresis. The final results are shown in Table 3.

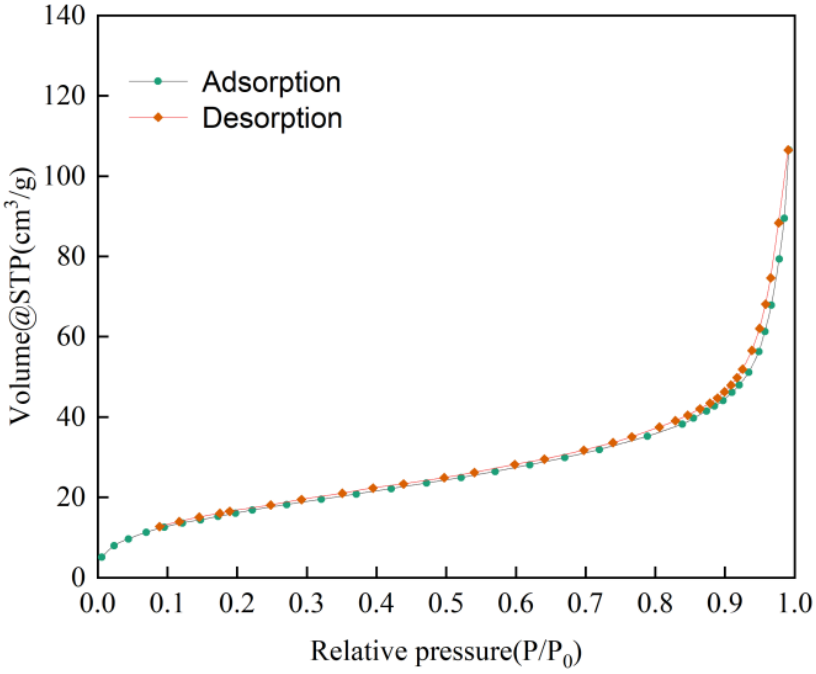

Figure 2. Nitrogen adsorption–desorption isotherms of D301 resin.

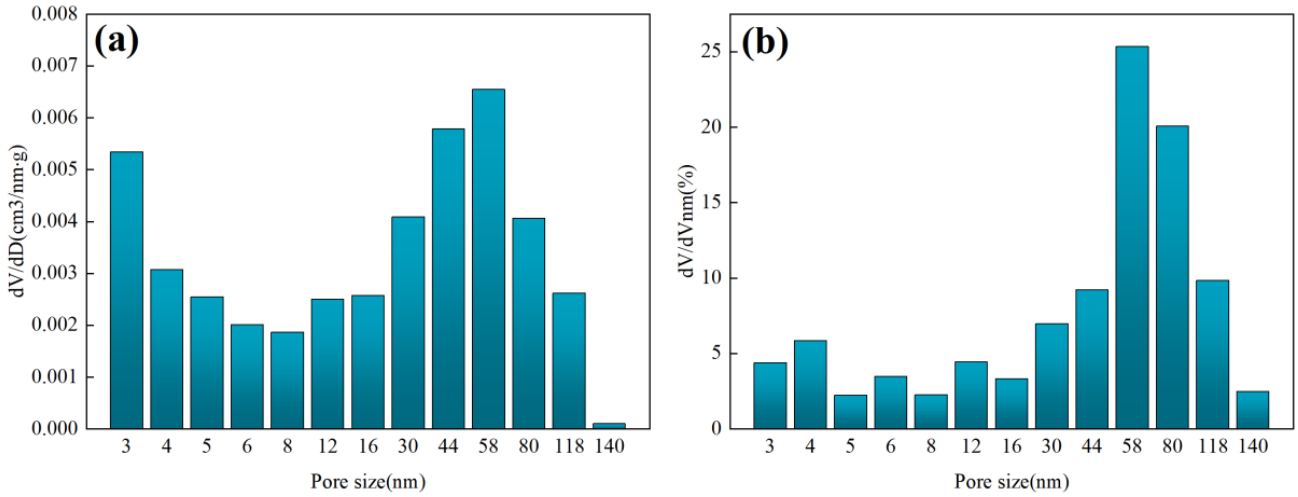

Figure 3. (**a**) Pore size distribution; (**b**) pore size distribution of relative total pore volume.

Table 3. Structural characteristics.

Resins	Surface Area^{BET} (m^2 g^{-1})	Pore Volume (cc g^{-1})	Average Pore Diameter (nm)
D301	45.31	0.3952	56.26
D301F	38.62	0.3563	63.43
D303	29.85	0.1542	40.37
D201	16.79	0.1467	52.1

The catalytic activity of the catalysts was compared with the most important properties of the resin: specific surface, average pore size, exchange capacity and functional groups. The results in Tables 2 and 3 show that the catalytic activity of all samples depends on their specific surfaces. This is less related to ion-exchange capacity, probably because ion-exchange capacity is a convenient feature of liquid phase processes in which the polymer

matrix expands so that all catalyst activity centers are available. The catalysis of the reactions in the gas phase is limited only by the base groups available on the resin surface, which increase with increasing specific surface area.

3.2.2. TG Analysis

Thermogravimetric analysis results of D301, D301F, D303 and D201 resins under nitrogen conditions are given in Figure 4. It can be seen that the weakly basic resins' weight loss trends are the same. The first mass plateau period occurs when the temperature increases from 50 to 150 °C without a significant decrease in catalyst mass. From 150 to 250 °C, a significant loss of catalyst mass begins to occur, followed by a second mass plateau period. The mass loss in the two plateau periods was almost 4.5% of the overall mass, which is close to the ratio of the mass of the tertiary amine group to the overall mass of the resin. Next, the content of amine groups on the surface of the weakly basic resins D301, D301F, and D303 was measured using the method described in Section 2.4. The results in Table 4 show that the amine content of the resin decreases when the heating temperature exceeds 150 °C. The mass of D201 resin decreases significantly from 100 °C, which indicates that weakly basic groups are more thermally stable than strongly basic groups. In fact, quaternary ammonium groups are prone to Hofmann decomposition at high temperatures [32]. The rapid decrease in the resin quality from 380 °C can be confirmed by the breakage of the styrene–divinylbenzene skeleton and the rapid decomposition after the generation of benzene derivatives.

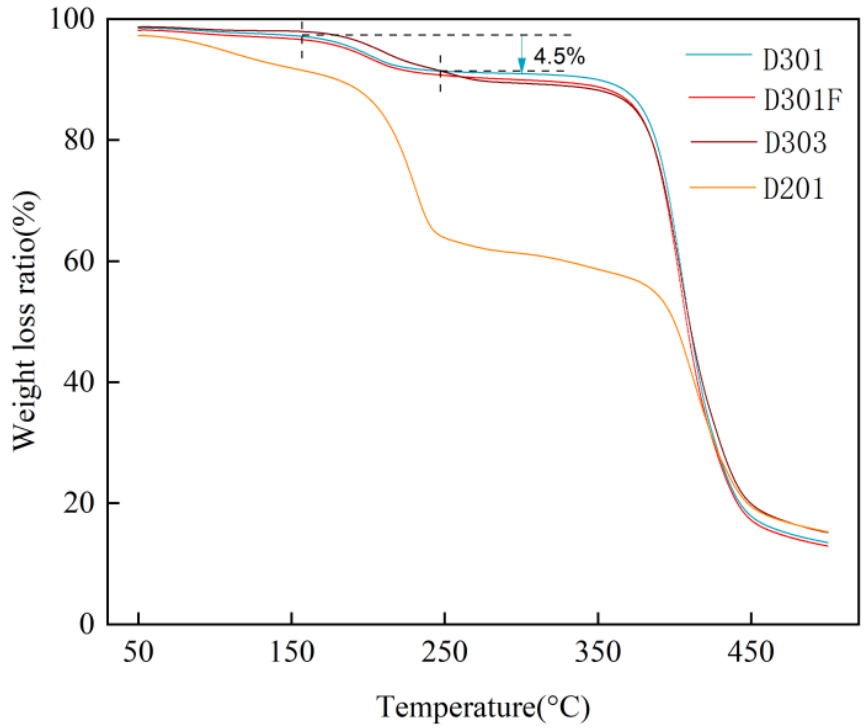

Figure 4. Thermogravimetric Analysis.

Table 4. Surface amine group content of weakly basic ion-exchange resins at different temperatures.

T/°C	120	130	140	150	160
D301	4.499%	4.893%	4.473%	4.160%	3.26%
D301F	4.450%	4.655%	4.363%	3.945%	3.272%
D303	4.285%	4.503%	4.348%	4.043%	3.023%

3.2.3. SEM and TEM Analysis

As shown in Figure 5b, all resin catalysts are homogeneous spheres with a relatively rough surface having many capillary pores. At the same time, the interior is loose and porous with a well-developed pore structure (Figure 5c), which allows reactants and products to diffuse rapidly inside the resin. The internal structural characteristics of the resins used were similar, differing in specific surface area, pore space and pore size, consistent with the pore properties results obtained by N_2 adsorption and desorption.

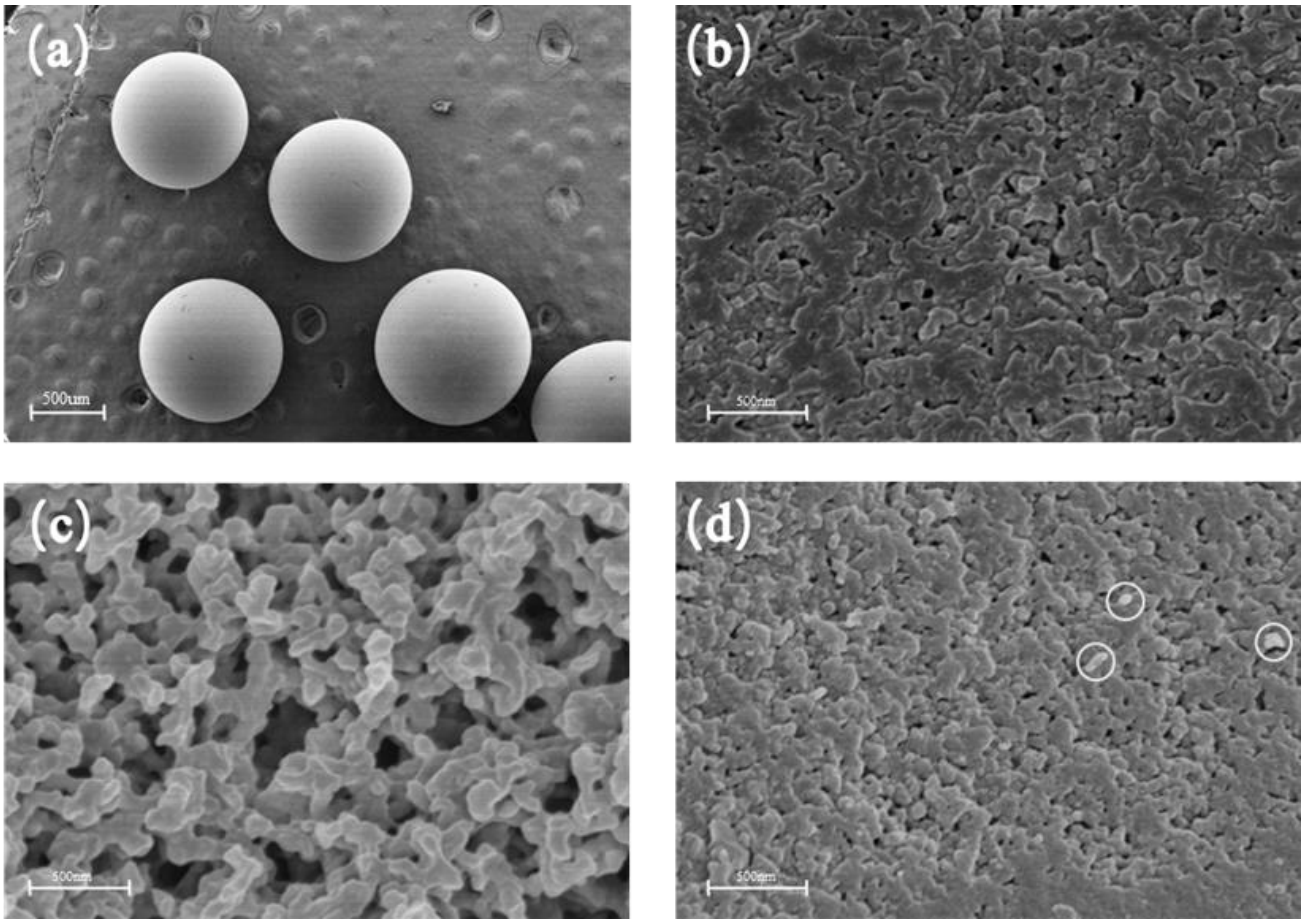

Figure 5. SEM micrographs of D301 resin: (**a**) resin shape; (**b**) resin surface before reaction; (**c**) resin internal structure before reaction; (**d**) resin surface after reaction.

Figure 5d shows SEM images of a resin surface after the reaction. The pore size of some capillaries on the resin surface became significantly smaller, and obvious lumpy particles (circled in Figure 5d) appeared on the resin surface. This phenomenon indicates that during the reaction process, silica powder may have been generated as a byproduct and adhered to the catalyst surface [19]. Similarly, in the study of the acylation reaction of diphenyl ether with acetic anhydride catalyzed by the resin Amberlyst 36, Yadav et al. [33] also found that the activity of the resin decreased in subsequent reactions due to the blockage of the pores by larger products.

Figure 6 shows the distribution of carbon, nitrogen, and oxygen elements on the D301 resin surface. Carbon, nitrogen, and oxygen are relatively uniformly distributed without significant aggregation, indicating that the active centers are uniformly distributed inside the catalyst.

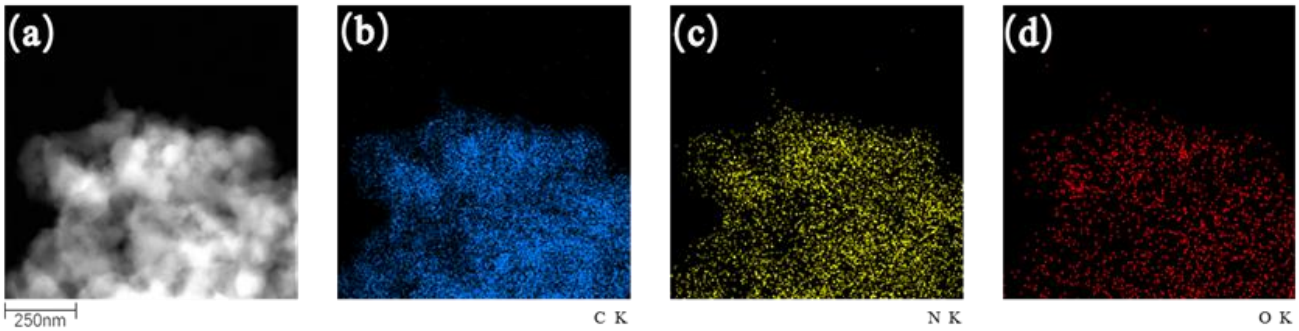

Figure 6. (**a**) TEM image of D301 resin; EDS mapping images show the distribution of carbon (**b**), nitrogen (**c**), oxygen (**d**).

3.2.4. XRD Analysis

After one week of continuous reaction in the reactor, the resins used for the catalytic reaction were analyzed by XRD, and the results are shown in Figure 7. The XRD signals of the fresh and used resins are different. In the XRD images of the resins after the reaction, a faint narrow peak appears at 28.44°, which is consistent with the standard XRD card for silicon (Si). The peak can be attributed to the crystalline surface of silicon (111), indicating that a small amount of byproduct silicon was produced in the reaction. According to the reports [19,34], silicon may originate from the process described in Equations (4) and (5): trace amounts of $SiHCl_3$ in the reaction products are dechlorinated to form silicon dichloride ($SiCl_2$), followed by disproportionation of $SiCl_2$ to form Si. Therefore, silicon may accumulate on the resin surface and in the pore channels over a long period of time. This result is also consistent with the SEM images of the resin surface after the reaction. Since this reaction has a slow reaction rate, silicon powder does not accumulate significantly on the resin even if the reaction is carried out for a long time, resulting in lower peak intensity in the XRD patterns.

$$SiHCl_3 \rightleftharpoons SiCl_2 + HCl \quad (4)$$

$$2SiCl_2 \rightleftharpoons Si + SiCl_4 \quad (5)$$

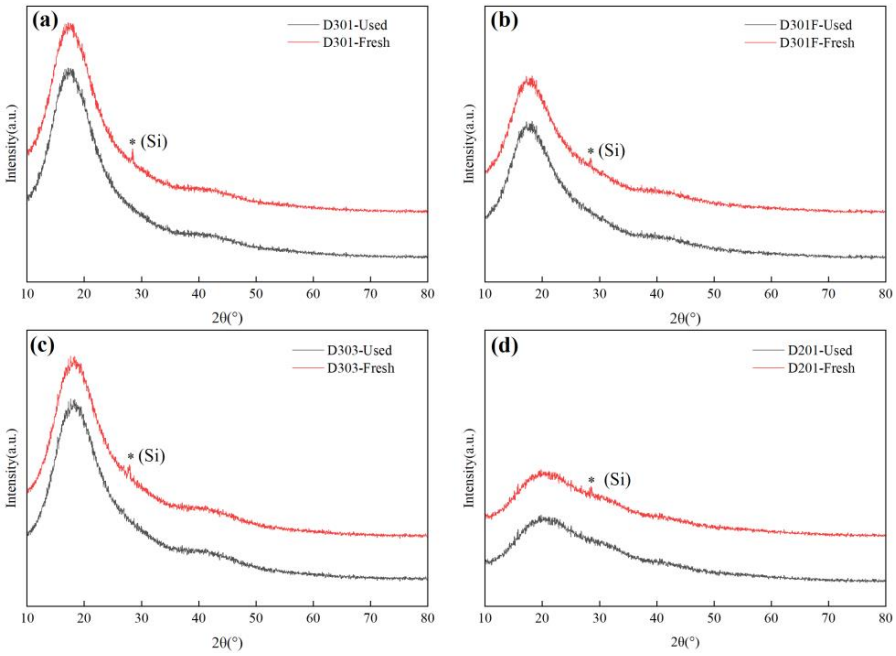

Figure 7. XRD patterns of resins before and after reaction: (**a**) D301 resin; (**b**) D301F resin; (**c**) D303 resin; (**d**) D201 resin. (Absorption peak from Silicon is indicated by the asterisk).

3.3. Reaction Characterization

In order to determine the optimal process conditions, we investigated the effects of reaction temperature, reactant ratio, and LHSV on catalytic effect and catalyst stability. D301 resin was selected for further characterization of the CH_3SiHCl_2 reaction due to its better catalytic performance and thermal stability. The final results are shown in Figure 8.

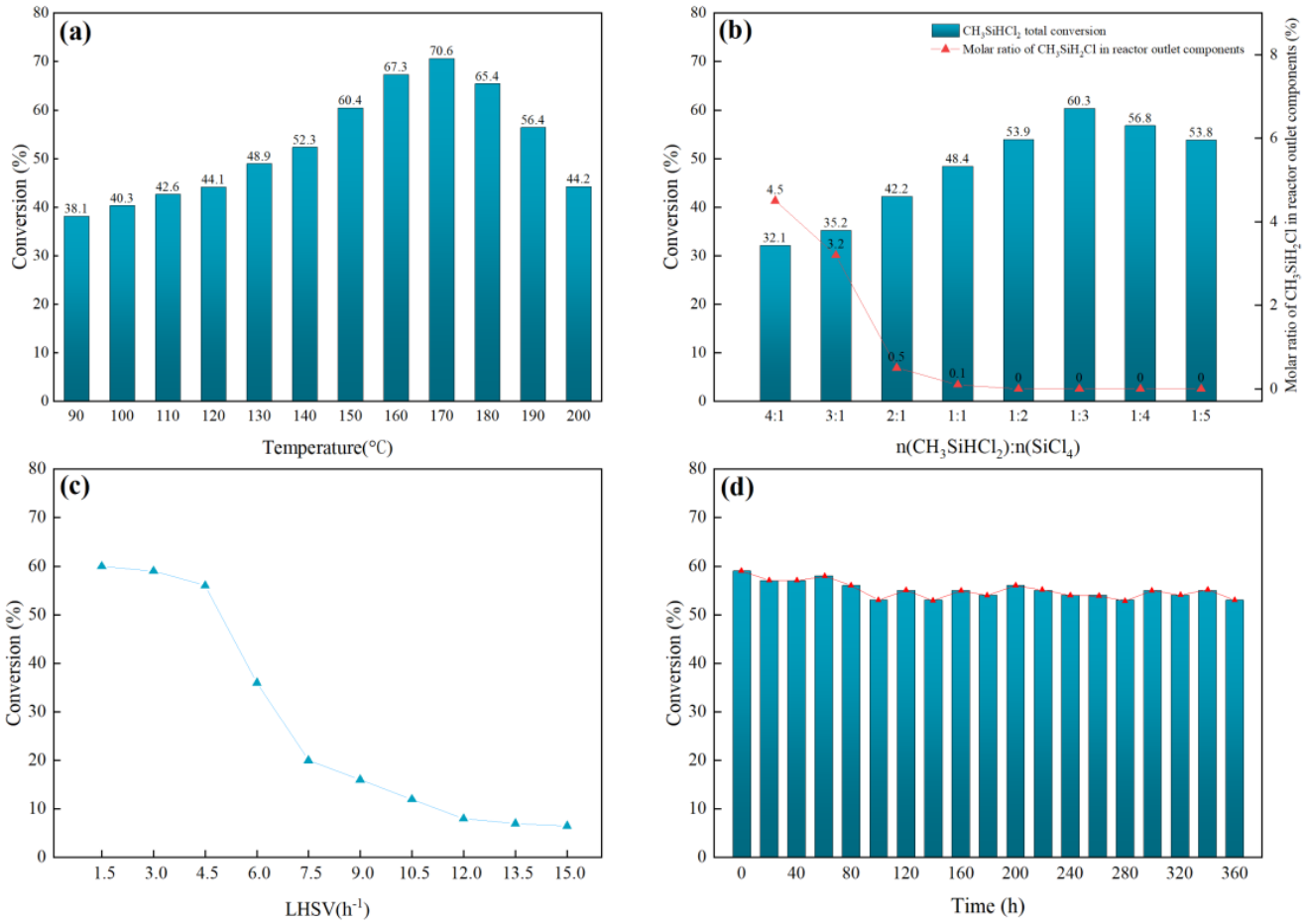

Figure 8. (**a**) The effect of temperature on the activity of the D301 resin; (**b**) the effect of reactant molar ratio on the activity of the D301 resin; (**c**) the effect of liquid hourly space velocity (LHSV) on the activity of the D301 catalyst; (**d**) results of the catalytic reaction of D301 resin at 150 °C in 360 h.

3.3.1. Effect of Temperature on CH_3SiHCl_2 Conversion

In general, the reaction temperature has a significant effect on the reaction rate. The study was carried out at different reaction temperatures, e.g., from 90, 100, 110, up to 200 °C, with an LHSV of 1.5 h^{-1} and n(CH_3SiHCl_2):n($SiCl_4$) = 1:3.

Figure 8a shows that the conversion of CH_3SiHCl_2 increases with increasing temperature. The conversion rate of CH_3SiHCl_2 was highest at 170 °C. After that, the conversion of CH_3SiHCl_2 decreased rapidly with increasing temperature. However, the forward reaction theoretically releases heat, and increasing the temperature should inhibit the reaction. This result can be explained by the fact that the Si-Cl bond dissociation energy of $SiCl_4$ is as high as 377 KJ/mol [19]. Although CH_3SiHCl_2 can lower the binding energy as a reducing agent, the reaction process is far from equilibrium at lower temperature and the reaction rate accelerates with increasing temperature. As the temperature continued to increase, the overall conversion rate decreased due to the decrease in equilibrium constant and degradation of the resin functional groups at high temperature. The results show that temperature significantly affects the conversion effect. Considering the service life of the resin, the optimal reaction temperature was set to 150 °C in subsequent tests.

3.3.2. Effect of Reactant Ratio on CH_3SiHCl_2 Conversion

The effect of the molar ratio of CH_3SiHCl_2 and $SiCl_4$ on the catalytic effect was investigated at a reaction temperature of 150 °C and an LHSV of 3 h^{-1}. As can be seen in Figure 8b, when n(CH_3SiHCl_2):n($SiCl_4$) is 4:1, the conversion of CH_3SiHCl_2 exceeds 25% (theoretical maximum conversion). This is due to the disproportionation reaction (Equation (6)) of excess CH_3SiHCl_2 increasing conversion. The existence of the reaction was subsequently confirmed by catalyzing pure CH_3SiHCl_2 with a weakly basic anion-exchange resin.

$$CH_3SiHCl_2 \rightleftharpoons CH_3SiH_2Cl + CH_3SiCl_3 \quad (6)$$

As the molar proportion of $SiCl_4$ in the system increased, the reaction equilibrium shifted to the right, and the conversion of CH_3SiHCl_2 increased while the proportion of CH_3SiH_2Cl in the reaction system gradually decreased. The content of CH_3SiH_2Cl decreased to the point that it was difficult to detect in the chromatography when the n(CH_3SiHCl_2):n($SiCl_4$) was 1:2. The conversion of CH_3SiHCl_2 reached the maximum (60.3%) when the molar proportion of $SiCl_4$ in the system increased to 1:3, and the conversion of CH_3SiHCl_2 showed a decreasing trend when the molar proportion of $SiCl_4$ in the system continued to increase, which was probably due to the CH_3SiHCl_2 concentration on the surface of the catalyst active center offsetting the above effect.

3.3.3. Effect of Reaction Liquid Hourly Space Velocity (LHSV) on CH_3SiHCl_2 Conversion

In the catalytic process, LHSV is the critical parameter of catalyst treatment capacity. The experiments were carried out by varying LHSV between 1.5 h^{-1} and 15 h^{-1} and keeping the molar ratio of $SiCl_4$ to CH_3SiHCl_2 at 3 at 150 °C. The effect of LHSV on the catalytic reaction can be seen in Figure 8c. When LHSV was less than 3 h^{-1}, the conversion rate did not decrease further. However, when LHSV was greater than 3 h^{-1}, the conversion decreased rapidly with the increase of LHSV. The catalytic conversion rate decreased from 59.80% to 6.81% when LHSV was increased from 3h^{-1} to 15h^{-1}. The CH_3SiHCl_2 conversion rate decrease was attributed to the decrease of relative active centers with increasing treatment volume. From the viewpoint of economy and treatment effectiveness, an LHSV of 3 h^{-1} was selected as the appropriate treatment volume for the whole system.

3.3.4. Catalytic Stability

An increase in reaction temperature improves the conversion rate of CH_3SiHCl_2, but a reaction temperature over 150 °C causes the functional group to be partially decomposed. In order to investigate the stability of D301 resin during a long reaction, D301 samples were observed for 360 h at a $SiCl_4$ to CH_3SiHCl_2 molar ratio of 3. It can be seen from Figure 8d that the catalytic effect of the D301 resin at 150 °C varied very little over time, but long-term use caused the catalytic activity to decrease. This may be due to the small amount of silica powder attached to the resin surface, which hinders contact between the reactants and the active center and reduces catalytic efficiency.

3.4. Possible Pathways for Resin Catalysts to Drive the Conversion of CH_3SiHCl_2 to CH_3SiCl_3

According to Union Carbide, $SiHCl_3$ forms a complex [RMe2NHSiCl3] with the amine group of a resin in the presence of a weakly basic resin catalyst [35], while Andrey V. Vorotyntsev [36] demonstrated the protonation of the nitrogen atom in the pyridine ring upon exposure to HCl or $SiHCl_3$ and the simultaneous formation of $N^+H\cdots Cl^-/N^+H\cdots SiCl_3{}^-$. In pre-experiments, it was also confirmed that CH_3SiHCl_2 undergoes the first step of disproportionation to form CH_3SiH_2Cl and CH_3SiCl_3, the amount of CH_3SiH_2Cl disproportionation being negligible. However, the results in Figure 8b show that after introducing $SiCl_4$ into the reaction system, the molar ratio of CH_3SiH_2Cl decreased rapidly. Therefore, the reaction of CH_3SiHCl_2 with $SiCl_4$ will proceed simultaneously as shown in Figure 9I,II.

I.

$$2CH_3SiHCl_2 \rightleftharpoons CH_3SiH_2Cl + CH_3SiCl_3$$

$$CH_3SiH_2Cl + SiCl_4 \rightleftharpoons CH_3SiHCl_2 + SiHCl_3$$

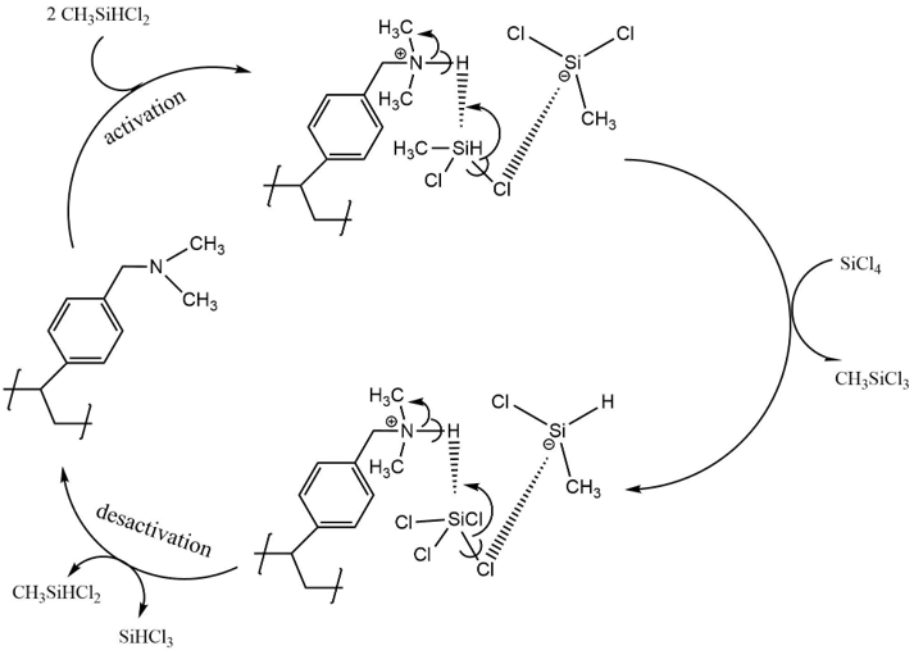

II.

$$CH_3SiHCl_2 + SiCl_4 \rightleftharpoons CH_3SiCl_3 + SiHCl_3$$

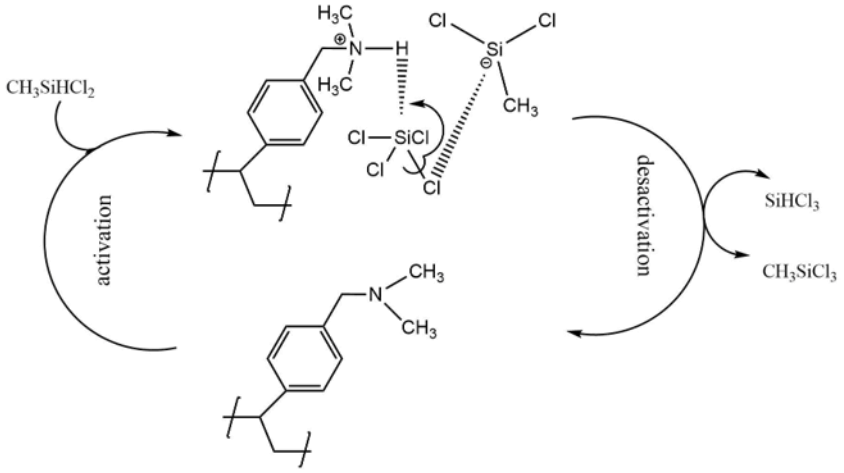

Figure 9. Catalytic mechanism of the reaction between CH_3SiHCl_2 and $SiCl_4$ on D301 resin.

In Figure 9I, in the first step, a CH_3SiHCl_2 molecule is adsorbed to the resin's active center, which leads to the formation of $CH_3SiCl_2^-$ and N-H^+. In the second step, the chlorine atom on a new CH_3SiHCl_2 molecule attacks the silicon atom on $CH_3SiCl_2^-$ to form CH_3SiCl_3, while the N-H bond breaks to form CH_3SiH_2Cl. In the third step, the newly generated CH_3SiH_2Cl is also adsorbed to the resin's active center, forming CH_3SiHCl^- and N-H^+. Finally, the chlorine atom on a $SiCl_4$ molecule attacks the silicon atom on CH_3SiHCl^- to form CH_3SiHCl_2, while the N-H bond is broken to form $SiHCl_3$. The presence of CH_3SiH_2Cl in the product illustrates the possibility of this process. In Figure 9II, after activation of the resin molecule by CH_3SiH_2Cl, the chlorine atom of a $SiCl_4$ molecule directly attacks the silicon atom on $CH_3SiCl_2^-$, and the products CH_3SiCl_3 and $SiHCl_3$ are

obtained. The probability of contact between the two is low when the content of CH_3SiHCl_2 is much larger than that of $SiCl_4$ after the functional group of the resin adsorbs CH_3SiHCl_2. The reaction of CH_3SiHCl_2 with $SiCl_4$ proceeds as shown in Figure 9I. When $SiCl_4$ is in excess, both react primarily in the reaction pathway shown in Figure 9II.

4. Conclusions

In this work, we studied a new method for removing carbon impurities (CH_3SiHCl_2) in $SiHCl_3$. $SiCl_4$ is used as a chlorinating agent to convert low-boiling-point CH_3SiHCl_2 into high-boiling-point CH_3SiCl_3 with an anion-exchange resin. The resin was characterized by BET, TG, SEM/TEM and XRD, and the temperature stability of the catalyst was determined by chemical analysis.

Among various ion-exchange resins, D301 macroporous resin has the best catalytic effect. It catalyzes the conversion of CH_3SiHCl_2 to CH_3SiCl_3 under the following conditions: n ($SiCl_4$):n (CH_3SiHCl_2) = 3:1, reaction temperature 150 °C, and LHSV 3 h^{-1}, with optimal conversion of CH_3SiHCl_2 being close to 60%. Finally, based on the comparison of reaction products, possible intermediate reaction processes and reaction mechanisms were investigated.

The characterization results show that a weakly basic anion-exchange resin has better thermal stability than a strongly basic anion-exchange resin. When the temperature exceeds 150 °C, the loss of the tertiary amine group of a weakly basic anion-exchange resin causes the reduction of catalytic activity. The large specific surface area and developed pore structure of the resin facilitate the diffusion of reactants and products in the pores. A small amount of silica powder will be produced during the reaction. Long-term accumulation of silica powder in the resin pore channel may reduce the catalytic efficiency of the resin.

Furthermore, the research results show that the weakly basic anion-exchange resin has the advantages of low cost and high activity, and has clear applicability for the catalytic conversion of CH_3SiHCl_2 to CH_3SiCl_3.

Author Contributions: Resources, validation, M.Z.; investigation, data curation, writing—original draft preparation, writing—review and editing, J.L.; supervision, project administration, funding acquisition, G.H. All authors have read and agreed to the published version of the manuscript.

Funding: This research received no external funding.

Data Availability Statement: Not applicable.

Conflicts of Interest: The authors declare no conflict of interest.

References

1. Haegel, N.M.; Atwater, H.; Barnes, T.; Breyer, C.; Burrell, A.; Chiang, Y.-M.; De Wolf, S.; Dimmler, B.; Feldman, D.; Glunz, S.; et al. Terawatt-Scale Photovoltaics: Transform Global Energy. *Science* **2019**, *364*, 836–838. [CrossRef] [PubMed]
2. Braga, A.F.B.; Moreira, S.P.; Zampieri, P.R.; Bacchin, J.M.G.; Mei, P.R. New Processes for the Production of Solar-Grade Polycrystalline Silicon: A Review. *Sol. Energy Mater. Sol. Cells* **2008**, *92*, 418–424. [CrossRef]
3. Irikura, K.; Muroi, M.; Yamada, A.; Matsuo, M.; Habuka, H.; Ishida, Y.; Ikeda, S.I.; Hara, S. Advantages of a Slim Vertical Gas Channel at High SiHCl3 Concentrations for Atmospheric Pressure Silicon Epitaxial Growth. *Mater. Sci. Semicond. Process.* **2018**, *87*, 13–18. [CrossRef]
4. Wang, S.H.; Chang, H.E.; Lee, C.C.; Fuh, Y.K.; Li, T.T. Evolution of A-Si:H to Nc-Si:H Transition of Hydrogenated Silicon Films Deposited by Trichlorosilane Using Principle Component Analysis of Optical Emission Spectroscopy. *Mater. Chem. Phys.* **2020**, *240*, 122186. [CrossRef]
5. Ran, Y.; Wang, J.; Yin, Y. Theoretical Study on the SiH 4 À n Cl n (n = 0–4) Reaction Mechanisms for Polysilicon Production Process. *Comput. Theor. Chem.* **2014**, *1035*, 60–67. [CrossRef]
6. Hou, Y.Q.; Xie, G.; Nie, Z.F.; Li, N. Direct Current Heating Model for the Siemens Reactor. *Adv. Mater. Res.* **2014**, *881–883*, 1805–1808. [CrossRef]
7. Vorotyntsev, A.V.; Mochalov, G.M.; Vorotyntsev, V.M. Kinetics of Catalytic Hydrogen Reduction of SiCl4 in the Presence of Nickel Chloride. *Inorg. Mater.* **2013**, *49*, 1–5. [CrossRef]
8. Nie, Z.; Wang, Y.; Wang, C.; Guo, Q.; Hou, Y.; Ramachandran, P.A.; Xie, G. Mathematical Model and Energy Efficiency Analysis of Siemens Reactor with a Quartz Ceramic Lining. *Appl. Therm. Eng.* **2021**, *199*, 117522. [CrossRef]

9. Seigneur, H.; Mohajeri, N.; Brooker, R.P.; Davis, K.O.; Schneller, E.J.; Dhere, N.G.; Rodgers, M.P.; Wohlgemuth, J.; Shiradkar, N.S.; Scardera, G.; et al. Manufacturing Metrology for C-Si Photovoltaic Module Reliability and Durability, Part I: Feedstock, Crystallization and Wafering. *Renew. Sustain. Energy Rev.* **2016**, *59*, 84–106. [CrossRef]
10. Lee, J.Y.; Lee, W.H.; Park, Y.K.; Kim, H.Y.; Kang, N.Y.; Yoon, K.B.; Choi, W.C.; Yang, O.B. Catalytic Conversion of Silicon Tetrachloride to Trichlorosilane for a Poly-Si Process. *Sol. Energy Mater. Sol. Cells* **2012**, *105*, 142–147. [CrossRef]
11. Desenfant, A.; Laduye, G.; Vignoles, G.L.; Chollon, G. Kinetic and Gas-Phase Study of the Chemical Vapor Deposition of Silicon Carbide from C2H3SiCl3/H2. *J. Ind. Eng. Chem.* **2021**, *94*, 145–158. [CrossRef]
12. Zhang, H.; Lu, P.; Ding, Z.; Li, Y.; Li, H.; Hua, C.; Wu, Z. Design Optimization and Control of Dividing Wall Column for Purification of Trichlorosilane. *Chem. Eng. Sci.* **2022**, *257*, 117716. [CrossRef]
13. Díez, E.; Rodríguez, A.; Gómez, J.M.; Olmos, M. Distillation Assisted Heat Pump in a Trichlorosilane Purification Process. *Chem. Eng. Process. Process Intensif.* **2013**, *69*, 70–76. [CrossRef]
14. Long, N.V.D.; Kwon, Y.; Lee, M. Design and Optimization of Thermally Coupled Distillation Schemes for the Trichlorosilane Purification Process. *Appl. Therm. Eng.* **2013**, *59*, 200–210. [CrossRef]
15. Boukherroub, R.; Chatgilialoglu, C.; Manuel, G. PdCl2-Catalyzed Reduction of Organic Halides by Triethylsilane. *Organometallics* **1996**, *15*, 1508–1510. [CrossRef]
16. Yamamoto, Y.; Materials, S. Synthesis of Chlorosilanes from (Fluoroalkyl)silanes, Bis(silyl)benzenes, and.alpha.,.omega.-Dihydropolysiloxanes. *Organometallics* **1994**, *13*, 808–812.
17. Wan, Y.; Liu, J.; Mao, Q.; Chang, X.; Song, Y.; Yuan, Z.; You, Z.; Zhao, X.; Tian, J.Z.; Yan, D.; et al. Exploration of Photocatalytic Chlorination Combined Simplified Distillation to Produce Electronic Grade High-Purity Trichlorosilane via Microchannel Reactor Experiments, Multiphase-Flow Simulation, ReaxFF MD, and DFT. *Chem. Eng. J.* **2022**, *450*, 138020. [CrossRef]
18. Liu, T.; Wang, T.; Huang, Y.; Wang, C.; Wang, J. Detailed Kinetics of Methylphenyldichlorosilane Synthesis from Methyldichlorosilane and Chlorobenzene by Gas Phase Condensation. *Chin. J. Chem. Eng.* **2015**, *23*, 954–961. [CrossRef]
19. Ivanov, V.M.; Trubitsin, Y.V. Approaches to Hydrogenation of Silicon Tetrachloride in Polysilicon Manufacture. *Russ. Microelectron.* **2011**, *40*, 559–561. [CrossRef]
20. Cho, Y.S.; Han, J.S.; Yoo, B.R.; Kang, S.O.; Jung, I.N. Palladium-Catalyzed Selective Dechlorination of Polychloromethylsilanes with Trichlorosilane. *Organometallics* **1998**, *17*, 570–573. [CrossRef]
21. Ferreira, R.S.B.; Bejarano-Alva, I.J.; Shimamoto, G.G.; Tubino, M.; Meirelles, A.J.A.; Batista, E.A.C. Optimizing the Production of Biodiesel from Palm Olein (Elaeis Guineensis Jacq.) Using a Strong Basic Anionic Resin as a Heterogeneous Catalyst. *Ind. Crops Prod.* **2021**, *174*, 114121. [CrossRef]
22. Medina-Herrera, N.; Tututi-Avila, S.; Jiménez-Gutiérrez, A.; Segovia-Hernández, J.G. Optimal Design of a Multi-Product Reactive Distillation System for Silanes Production. *Comput. Chem. Eng.* **2017**, *105*, 132–141. [CrossRef]
23. Yasukouchi, H.; Machida, K.; Nishiyama, A.; Mitsuda, M. Efficient and Practical Deacylation Reaction System in a Continuous Packed-Bed Reactor. *Org. Process Res. Dev.* **2019**, *23*, 654–659. [CrossRef]
24. Laroche, B.; Saito, Y.; Ishitani, H.; Kobayashi, S. Basic Anion-Exchange Resin-Catalyzed Aldol Condensation of Aromatic Ketones with Aldehydes in Continuous Flow. *Org. Process Res. Dev.* **2019**, *23*, 961–967. [CrossRef]
25. Sasayama, T.; Hiromori, K.; Takahashi, A.; Shibasaki-Kitakawa, N. Process for Continuous Production of Sugar Esters of Medium-Chain Fatty Acid: Effect of Residence Time on Productivity and Scale-up Design. *J. Food Eng.* **2021**, *305*, 110608. [CrossRef]
26. Wu, H.S.; Lee, C.S. Catalytic Activity of Quaternary Ammonium Poly(Methylstyrene-Co-Styrene) Resin in an Organic Solvent/Alkaline Solution. *J. Catal.* **2001**, *199*, 217–223. [CrossRef]
27. Li, Y.; Yu, F.; He, W.; Yang, W. The Preparation and Catalytic Performance of Graphene-Reinforced Ion-Exchange Resins. *RSC Adv.* **2015**, *5*, 2550–2561. [CrossRef]
28. Mori, K.; Dojo, M.; Yamashita, H. Pd and Pd-Ag Nanoparticles within a Macroreticular Basic Resin: An Efficient Catalyst for Hydrogen Production from Formic Acid Decomposition. *ACS Catal.* **2013**, *3*, 1114–1119. [CrossRef]
29. Sasayama, T.; Kamikanda, Y.; Shibasaki-Kitakawa, N. Process Design for Green and Selective Production of Bio-Based Surfactant with Heterogeneous Resin Catalyst. *Chem. Eng. J.* **2018**, *334*, 2231–2237. [CrossRef]
30. Maia Filho, D.C.; Salim, V.M.M.; Borges, C.P. Membrane Contactor Reactor for Transesterification of Triglycerides Heterogeneously Catalyzed. *Chem. Eng. Process. Process Intensif.* **2016**, *108*, 220–225. [CrossRef]
31. Liu, T.-T.; Ma, C.-H.; Sui, X.-Y.; Yang, L.; Zu, Y.-G.; Zhao, C.-J.; Li, C.-Y.; Zhang, L. Preparation of Shikonin by Hydrolyzing Ester Derivatives Using Basic Anion Ion Exchange Resin as Solid Catalyst. *Ind. Crops Prod.* **2012**, *36*, 47–53. [CrossRef]
32. Tianshu, B.; Lixuan, Z.; Chunhong, W. The Synthesis of Thermostable, Strongly Basic Anion-Exchange Resins Using Cross-Linked Biguanide and Its Application in the Extraction of Sodium Copper Chlorophyllin. *J. Chromatogr. B* **2022**, *1211*, 123436. [CrossRef] [PubMed]
33. Yadav, G.D.; Nalawade, S.P. Selectivity Engineering of 4-Phenoxyacetophenone by Acylation of Diphenyl Ether with Ion Exchange Resins: Modeling of Catalyst Deactivation and Remedies. *Chem. Eng. Sci.* **2003**, *58*, 2573–2585. [CrossRef]
34. Ravasio, S.; Masi, M.; Cavallotti, C. Analysis of the Gas Phase Reactivity of Chlorosilanes. *J. Phys. Chem. A* **2013**, *117*, 5221–5231. [CrossRef] [PubMed]

35. Li, K.Y.; Huang, C.D. Redistribution Reaction of Trichlorosilane in a Fixed-Bed Reactor. *Ind. Eng. Chem. Res.* **1988**, *27*, 1600–1606. [CrossRef]
36. Vorotyntsev, A.V.; Petukhov, A.N.; Makarov, D.A.; Razov, E.N.; Vorotyntsev, I.V.; Nyuchev, A.V.; Kirillova, N.I.; Vorotyntsev, V.M. Synthesis, Properties and Mechanism of the Ion Exchange Resins Based on 2-Methyl-5-Vinylpyridine and Divinylbenzene in the Catalytic Disproportionation of Trichlorosilane. *Appl. Catal. B Environ.* **2018**, *224*, 621–633. [CrossRef]